catalysts

MDPI

Article

$LaFeO_3$ Modified with Ni for Hydrogen Evolution via Photocatalytic Glucose Reforming in Liquid Phase

Giuseppina Iervolino [1], Vincenzo Vaiano [1], Diana Sannino [1,*], Felipe Puga [2], Josè Antonio Navío [2] and María C. Hidalgo [2]

[1] Department of Industrial Engineering, University of Salerno, Via Giovanni Paolo II, 132, 84084 Fisciano, Italy; giiervolino@unisa.it (G.I.); vvaiano@unisa.it (V.V.)
[2] Instituto de Ciencia de Materiales de Sevilla (ICMS), Centro Mixto Universidad de Sevilla-CSIC, Américo Vespucio 49, 41092 Sevilla, Spain; felpugmar@alum.us.es (F.P.); navio@us.es (J.A.N.); mchidalgo@icmse.csic.es (M.C.H.)
* Correspondence: dsannino@unisa.it; Tel.: +39-089-964092; Fax: +39-089-964057

Abstract: In this work, the optimization of Ni amount on $LaFeO_3$ photocatalyst was studied in the photocatalytic molecular hydrogen production from glucose aqueous solution under UV light irradiation. $LaFeO_3$ was synthesized via solution combustion synthesis and different amount of Ni were dispersed on $LaFeO_3$ surface through deposition method in aqueous solution and using $NaBH_4$ as reducing agent. The prepared samples were characterized with different techniques: Raman spectroscopy, UltraViolet-Visible Diffuse Reflectance Spettroscopy (UV–Vis-DRS), X-ray Diffraction (XRD), X-ray Photoelectron Spectroscopy (XPS), X-ray Fluorescence (XRF), Transmission Electron microscopy (TEM), and Scanning Electron microscopy (SEM) analyses. For all the investigated photocatalysts, the presence of Ni on perovskite surface resulted in a better activity compared to pure $LaFeO_3$. In particular, it is possible to identify an optimal amount of Ni for which it is possible to obtain the best hydrogen production. Specifically, the results showed that the optimal Ni amount was equal to nominal 0.12 wt% (0.12Ni/$LaFeO_3$), for which the photocatalytic H_2 production was equal to 2574 μmol/L after 4 h of UV irradiation. The influence of different of photocatalyst dosage and initial glucose concentration was also evaluated. The results of the optimization of operating parameters indicated that the highest molecular hydrogen production was achieved on 0.12Ni/$LaFeO_3$ sample with 1.5 g/L of catalyst dosage and 1000 ppm initial glucose concentration. To determine the reactive species that play the most significant role in the photocatalytic hydrogen production, photocatalytic tests in the presence of different radical scavengers were performed. The results showed that •OH radical plays a significant role in the photocatalytic conversion of glucose in H_2. Moreover, photocatalytic tests carried out with D_2O instead of H_2O evidenced the role of water molecules in the photocatalytic production of molecular hydrogen in glucose aqueous solution.

Keywords: photocatalytic hydrogen; glucose; nickel; perovskite

Citation: Iervolino, G.; Vaiano, V.; Sannino, D.; Puga, F.; Navío, J.A.; Hidalgo, M.C. $LaFeO_3$ Modified with Ni for Hydrogen Evolution via Photocatalytic Glucose Reforming in Liquid Phase. *Catalysts* **2021**, *11*, 1558. https://doi.org/10.3390/catal11121558

Academic Editor: Vasile I. Parvulescu

Received: 10 November 2021
Accepted: 25 November 2021
Published: 20 December 2021

1. Introduction

For several decades, the use of hydrogen as an energy vector and not just as a raw material for the process industry was considered as a possible key element for the decarbonization of energy systems. The attention towards hydrogen was due to some of its interesting characteristics and, in particular, the possibility of using molecular hydrogen to produce "clean" energy. Indeed, the combustion of hydrogen is not associated with the production of carbon dioxide (CO_2) and, therefore, it does not involve direct climate-altering emissions. Until a few years ago, about 95% of hydrogen is obtained from fossil fuels starting from the steam reforming process and the remaining 5% from water by electrolysis. However, due to the depletion of not-renewable sources and the high amount of energy required, the production of molecular hydrogen through these two processes is unsustainable and uneconomical. To date, thanks to the development of

innovative technologies, molecular hydrogen can be obtained from a widely diversified range of renewable energy sources, thus being able to support the development of resilient energy systems [1,2]. Some recent advances in molecular hydrogen production indicate that a possible route is to perform cycloalkanes [3] and alcohol dehydrogenation [4] as green and sustainable method, but also to realize hydrolytic dehydrogenation of ammonia borane on reduced $CoFe_2O_4$ for the H_2 evolution [5] or the hydrolysis of $NaBH_4$ on ZIF-8 materials [6].

It is also possible to produce molecular hydrogen in a "clean" and renewable way with the application of a photocatalytic process. Already, typically used for the removal of organic contaminants from wastewater, the heterogeneous photocatalysis offers the opportunity to achieve molecular hydrogen production under the irradiation, by reforming of organic molecules in liquid phase. Indeed, in literature, it is reported that biomass photoreforming is a promising method for the molecular hydrogen production, not only because the method relies on predictably infinite solar energy inputs, but also it is based on a renewable biomass substrate and could use by-products of industrial biomass processes existing, e.g., ethanol from sugar fermentation [7,8]. The photoreforming process improves the well-known process of photocatalytic water-splitting [9] since the organic components acts as a hole scavengers, overcoming the main drawbacks of the water-splitting as unfavorable thermodynamics and rapid recombination of the O_2 and H_2 produced [10]. Sacrificial organics agents can be found in the wastewater: in particular, the characteristics of agri-food industry wastewater, which contains a high concentration of sugars, yield them suitable candidate for photoreforming process [11]. Cellulose behaves like a sacrificial agent through the depolymerization of cellulose into glucose products by oxidizing species and combines with the photo-generated oxidant species suppressing charge carrier recombination. In general, glucose represents one of the most efficient sacrificial substances for the photocatalytic production of hydrogen [8]. The photocatalytic production of hydrogen was studied for several years and there are many catalysts used for this purpose, such as TiO_2 based photocatalysts [12–15]. For example, a recent study reports the photocatalytic production of molecular hydrogen with TiO_2-based catalysts decorated with several metal nanoparticles (Ag, Co, Cr, Cu, Ni, Pd, Pt), starting from aqueous solutions containing an organic dye (brilliant green) [16]. Pd doped TiO_2 was used for molecular hydrogen production from ethanol aqueous solution [17]. Photocatalytic production of molecular hydrogen from methanol aqueous solutions using TiO_2/Pt/reduced graphene oxide composite was proposed by Rivero et al. [18]. The photocatalytic hydrogen production from glucose aqueous solution over TiO_2 modified by the simultaneous presence of fluorine and Pt (Pt-F-TiO_2) was reported in literature [19]. In this case fluorinated TiO_2 represents an interesting support for noble metals (Pt on TiO_2 surface) used in the photocatalytic hydrogen production from sugars in aqueous solution. In particular, fluorine significantly enhanced the photocatalytic H_2 production due to the formation of unbounded •OH radicals that are more reactive [20]. Pt is often used also as doping element for titania: in this case, Pt is a robust proton reduction catalyst and an increase in H_2 production under irradiation can be observed, as evidence of the suppression of electron–hole recombination [8]. About this, the photocatalytic molecular hydrogen evolution from cellulose with Pt/TiO_2 under visible light irradiation was studied [8]. Platinum is certainly one of the most performing elements to use (both on the surface and as a doping element), but it is also a very expensive noble metal. Less expensive than platinum, palladium was applied to dope TiO_2 or to modify its surface, resulting active in the photocatalytic hydrogen production both from water splitting and from biomass reforming [21]. For example Pd deposition on the TiO_2 surface was favorable for the photocatalytic H_2 and CH_4 production from glucose aqueous solution [22]. The wide application of noble metals in the photocatalytic production of hydrogen, involves also Au. In literature the in-situ photodeposition of Au metal on TiO_2 surface was studied for the photocatalytic hydrogen production from biomass solution [8,23]. Ni is cheaper than noble metals and could represent an alternative giving the interesting characteristics that have led to its use as cocatalyst combined with

semiconductors in photocatalytic processes. It is largely applied in the steam reforming process for the effectiveness in breaking the C−C, C−H, and C−O bonds [24]. Nickel species including metallic nickel [25], nickel oxides [26], nickel hydroxide [27], and nickel sulfide [28] were reported for the improving the photocatalytic activities [29]. Although TiO_2 based samples are the most studied and used photocatalyst for the photo-reforming reaction, there are interesting alternatives reported in several literature studies. For instance, perovskites, with typical ABO_3 structure where position A is occupied by the rare earth ion, and position B by the transition metal ion, were proposed as possible photocatalysts because they are semiconductors of lower band-gap with respect to the titania based, so easier to photoexcite [30]. Several studies were performed on $LaFeO_3$, one of the most common perovskites, which presents significant physical and chemical properties, attractive in several advanced technologies applications such as solid oxide fuel cells catalysts [31], chemical sensors [32], photocatalysis [33], and biosensors [34]. $LaFeO_3$ has attracted much attention in the photocatalysis due to its structural stability, abundance, non-toxicity and chemically stability. Several works in the literature report the efficiency of $LaFeO_3$ in the photocatalytic production of molecular hydrogen starting from aqueous solutions containing different types of organic substances, such as rhodamine B (RhB) [35], sucrose [36], glucose [11,20,37]. $LaFeO_3$ can be modified to improve its photocatalytic performance, and this can be done through the doping or surface modification with different types of noble or non-noble metals [37–41], or through the combination in composites [42,43]. For example, it is reported the use of Ru [44] and Rh [45] as dopant agents for $LaFeO_3$ in the photocatalytic molecular hydrogen production from glucose solutions. As a possible alternative to noble or other transition elements, the modification of $LaFeO_3$ surface with Ni could be interesting. Ni at optimal loading on TiO_2 has demonstrated to perform better than Au in photocatalytic hydrogen production [46] Moreover, relevant amount of molecular hydrogen was found on an Ni modified perovskite (Ni/La- $NaTaO_3$), at the optimal nickel load on the surface of the photocatalyst. Indeed the performances of the photocatalyst are strongly influenced by the Ni load tuning [47]. However, a recent literature paper reported the use of Ni with $LaFeO_3$ in the photocatalytic production of hydrogen [48] but the influence of Ni amount on photogenerated hydrogen was never studied. For this reason, given the interest in $LaFeO_3$, and given the particular properties of Ni for photocatalytic processes, Ni/$LaFeO_3$ catalyst for the photocatalytic production of molecular hydrogen starting from solutions containing glucose was studied in this paper. Additionally, to our knowledge, no detailed study of H_2 production from glucose solutions over Ni/$LaFeO_3$ photocatalysts was reported in the scientific literature, providing additional motivation for the current investigation. In particular, the aim of this work is to optimize the Ni loading dispersed on the $LaFeO_3$ surface, evaluate the effect of different operating parameters on molecular hydrogen production from glucose aqueous solution and propose a possible reaction mechanism.

2. Material and Methods

2.1. Synthesis of Photocatalysts

The procedure for the preparation of the catalysts tested during the experiments followed two subsequent steps. First of all, $LaFeO_3$ was prepared through the "solution combustion synthesis" method [49]. Specifically, citric acid as organic fuel and metal nitrate as metal precursor were used. Given amounts of $Fe(NO_3)_3{\cdot}9H_2O$ (Riedel-deHaen, 97 wt%), $La(NO_3)_3{\cdot}6H_2O$ (Fluka, 99%), and citric acid (Fluka, 99 wt%), were completely dissolved in 100 mL of distilled water. The solution was kept under continuous stirring at 60 °C. The pH of the solution was adjusted up to 7 by slow addition of ammonium hydroxide (Carlo Erba, 37 wt%). The solution was dried at 130 °C, and then calcined at 300 °C for 3 h to ignite the solution combustion reaction. Ni/$LaFeO_3$ photocatalysts were synthesized by a deposition method using $NaBH_4$ as reducing agent following the procedure proposed by Kaplan et al. [50]. For this scope, a suitable amount of $NiCl_2.6\ H_2O$ was added, obtaining

different sample with different Ni content. Specifically, the list of prepared samples is shown in Table 1.

Table 1. List of prepared photocatalysts.

Photocatalyst	Ni Nominal Amount [%wt]	$NiCl_2 \cdot 6\ H_2O$ Used in the Synthesis [g]	$LaFeO_3$ Used in the Synthesis [g]	Band Gap Energy Value [eV]
$LaFeO_3$	0	0	0.80	2.18
$0.06Ni/LaFeO_3$	0.06	0.004	1.60	2.18
$0.12Ni/LaFeO_3$	0.12	0.004	0.80	2.17
$0.18Ni/LaFeO_3$	0.18	0.006	0.80	2.17
$0.25Ni/LaFeO_3$	0.25	0.008	0.80	2.17

2.2. Photocatalysts Characterization

Different techniques were used to characterize the prepared photocatalysts. In particular the crystallite size and crystalline phase of photocatalysts were studied with an X-ray diffractometer (Assing), using Cu-Kα radiation. UV–vis reflectance spectra (UV-vis DRS) of powder catalysts were recorded by a Perkin Elmer spectrometer Lambda 35 using a RSA-PE-20 reflectance spectroscopy accessory (Labsphere Inc., North Sutton, NH, USA). All spectra were obtained using an 8° sample positioning holder, giving total reflectance relative to a calibrated standard SRS-010-99 (Labsphere Inc., North Sutton, NH, USA). Band-gap energy determinations of the photocatalysts were obtained from Kubelka–Munk function F(R∞) by plotting $[F(R\infty) \times h\nu]^2$ vs. $h\nu$. Transmission electron microscopy (TEM) was performed in a Philips CM 200 microscope. The samples for the microscopic analyzes were dispersed in ethanol using an ultrasonicator and dropped on a carbon grid. XPS analyses were performed with a Leybold–Heraeus LHS-10 spectrometer. A constant pass energy of 50 eV was employed. The main chamber was set at a pressure lower than 2×10^{-9} Torr. This equipment included an EA-200MCD hemispherical electron analyzer with a dual X-ray source working with Al Kα (hυ Ό 1486.6 eV) at 120 W and 30 mA. Adventitious C 1s signal located at 284.6 eV was used as internal energy reference. The samples were outgassed in the pre-chamber of the instrument at 150 °C up to a pressure below 2×10^{-8} Torr to remove chemisorbed water. The chemical composition of the samples was obtained by X-ray fluorescence spectrometry (XRF) using an AXIOS PANalytical spectrometer with Rh source of radiation. XRF measurements were performed onto pressed pellets (sample included in 10 wt% of wax). The Raman spectra of the samples were measured by a Dispersive Micro Raman system (Invia, Renishaw), equipped with 514 nm laser, in the range 200–2000 cm^{-1} Raman shift. Scanning electron microscopy (SEM) (Assing, mod. LEO 420) was used to characterize the morphology of the samples at an accelerating voltage of 20 kV.

2.3. Photocatalytic Tests

The performances of the prepared photocatalysts in terms of molecular hydrogen production were evaluated during photocatalytic tests under UV light irradiation using glucose aqueous solutions. In particular, the experiments were carried out in a cylindrical pyrex reactor (ID = 2.5 cm) equipped with a peristaltic pump necessary for the recirculation of the catalyst suspended in the reactor and for the continuous mixing of the glucose aqueous solution. A specific nitrogen flow rate (0.122 NL min^{-1}) is blown into the reactor, and it acts as a carrier for the gases produced during the reaction, and to yield the environment reducing. Four UV lamps (Philips TL 8W/08 F8 T5/BLB, nominal power of 8 W and emission peak at 365 nm) were used as light sources and positioned around the external surface of the reactor. Typically, 0.12 g of catalyst was suspended in 80 mL of aqueous solution containing 1,000 ppm of glucose (D+ Glucose VWR, Sigma-Aldrich). The suspension was left in dark conditions for 2 h to reach the adsorption-desorption equilibrium of glucose on the photocatalyst surface, and then the photocatalytic reaction was initiated under UV

light for up to 4 h. The analysis of the gaseous phase from the photoreactor was performed by a continuous CO_2, H_2, and CH_4 analyzers (ABB Advance Optima).

3. Results and Discussion

3.1. Photocatalysts Characterization

3.1.1. X-ray Diffraction (XRD)

Figure S1 showed the XRD patterns of the $LaFeO_3$ and 0.12Ni/$LaFeO_3$ sample. For both the samples, well indexed diffraction peaks were observed. This clearly indicates the formation of orthorhombic type perovskite structure for both prepared samples, with the higher intensity peak at 2θ value of 32.16, which corresponds to $LaFeO_3$ (0 0 2) crystalline plane, (JCPDS card No. 88-0641), as reported in literature [51]. The average crystallite size for these catalysts, calculated by Scherrer formula, is about 28 nm. No signals associated to Ni species were observed in the XRD spectra because of the very low Ni amount. This confirms that the presence of Ni on the $LaFeO_3$ surface, deposited by the reduction-impregnation method, does not affect the crystal structure of $LaFeO_3$.

3.1.2. UV-Vis Diffuse Reflectance Spectra

The Kubelka–Munk spectra of the samples $LaFeO_3$, 0.12Ni/$LaFeO_3$ and 0.25Ni/$LaFeO_3$ are shown in Figure 1a. The typical absorption band edges of the $LaFeO_3$ semiconductor were observed at around 814 and 600 nm for the prepared samples, attributed to electron transitions from valence band to conduction band (O2p→Fe3d). These two absorption band edge are especially noticeable for bare $LaFeO_3$ [52].

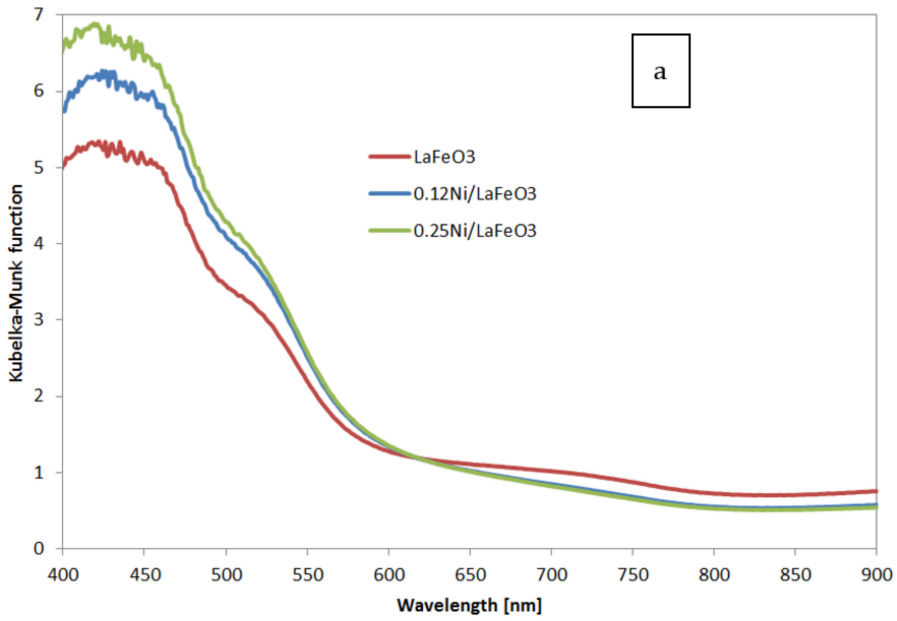

Figure 1. *Cont.*

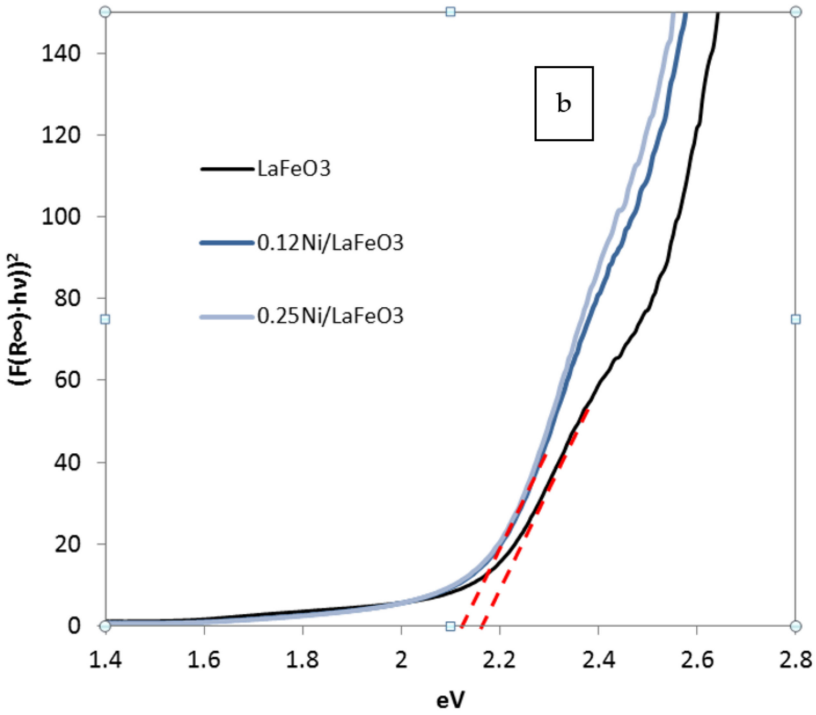

Figure 1. Kubelka–Munk function of $LaFeO_3$, 0.12 $Ni/LaFeO_3$, and 0.25$Ni/LaFeO_3$ photocatalysts (**a**). Band gap evaluation (**b**).

The presence of Ni mainly induces for $LaFeO_3$ photocatalysts an enhancement in the light absorptions in the UV-Vis region below 600 nm, that follows the Ni content [44]. It should point out that nickel nanoparticles don't exhibit relevant surface plasmon resonances because the polarizability of Ni (it possesses fewer free electrons) is weak than noble metals such as Au and Ag [53].The data obtained from UV–Vis reflectance spectra were used for evaluating the band-gap energy (Figure 1b). A band gap value of 2.18 eV is achieved for $LaFeO_3$ photocatalyst while a band gap value of about 2.17 eV was observed for 0.12$Ni/LaFeO_3$ and 0.25$Ni/LaFeO_3$ samples. The presence of Ni on the perovskite surface therefore induces only a slight modification in the band gap of the catalyst [48].

3.1.3. SEM Analysis

The morphology of the $LaFeO_3$ and $Ni/LaFeO_3$ photocatalysts was investigated by SEM microscopy and the obtained results are presented in Figure 2. For sake of brevity, together with $LaFeO_3$, only the analysis of 0.12$Ni/LaFeO_3$ photocatalyst is reported, being similar the results obtained for all the others $Ni/LaFeO_3$ samples. From the SEM images it is possible to observe flat particles with high degree of agglomeration. This agglomeration is induced by the particle-particle interactions. However, it is possible to clearly distinguish the porous structure of the catalyst, which confirms a material with low density. This type of result is due to the role of the fuel (citric acid) used during the synthesis which causes the combustion of the gel formed after drying. Specifically, the fuel, during combustion, releases a gas that comes out of the gel, breaking it and creating the final porous structure of the perovskite, both for $LaFeO_3$ and for the $Ni/LaFeO_3$ sample [44] The Ni doping in $LaFeO_3$ have a clear effect in the surface of the photocatalyst, since 0.12$Ni/LaFeO_3$ is more porous than $LaFeO_3$.

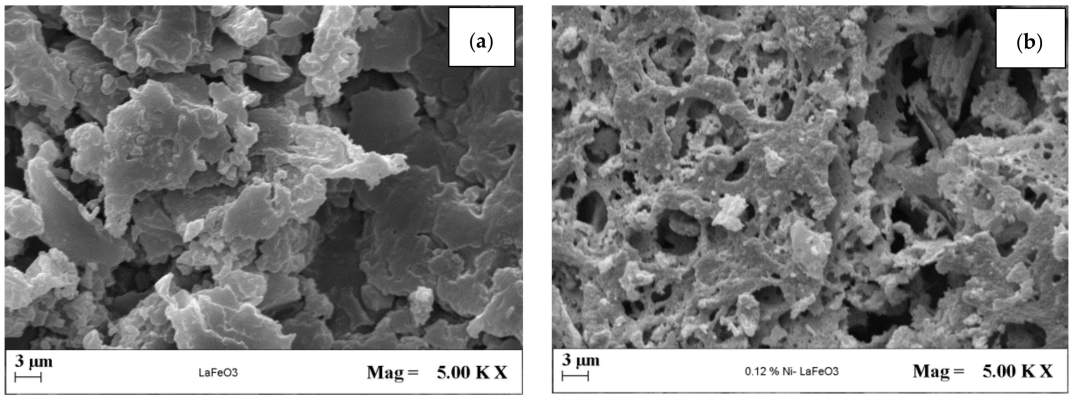

Figure 2. SEM images of $LaFeO_3$ (**a**) and 0.12 $Ni/LaFeO_3$ (**b**).

3.1.4. Raman Analysis

Raman spectra of the prepared photocatalysts are reported in Figure S2. All the samples showed bands in the range 100–700 cm^{-1}, all associated to $LaFeO_3$ structure [49]. The modes caused by La vibrations are present below 200 cm^{-1}, at 153 and 176 cm^{-1}. The bands in the range 400–450 cm^{-1} are due to the oxygen octahedral bending vibrations [54]. From the Raman results it is possible to observe that the Ni deposited on the surface of $LaFeO_3$ leaves similar signals to the spectrum of pristine perovskite.

3.1.5. TEM Analysis

Figure 3a shows the morphology of $LaFeO_3$, constituted by large aggregates less than 1000 nm and composed by almost rounded particles of lower dimensions, ranging from 100 nm to more than 200 nm. The observed nanoparticles appear distributed inside the larger grain, even if they are well evidenced at its border. Similar aggregate structure can be observed for 0.12 $Ni/LaFeO_3$ in Figure 3b, but the aggregate was found lower in the dimensions, in particular up to 500 nm. Nanoparticles of 100 nm and less, more irregular in shape were surrounded by little irregular amorphous layers. For 0.25$Ni/LaFeO_3$, reported in Figure 3c, nanoparticle aggregates less than 600 nm in size are observable, composed by irregular and not uniform nanoparticles ranging from about 100 nm to lower sizes. In the right-side image, some amorphous layer can be observed.

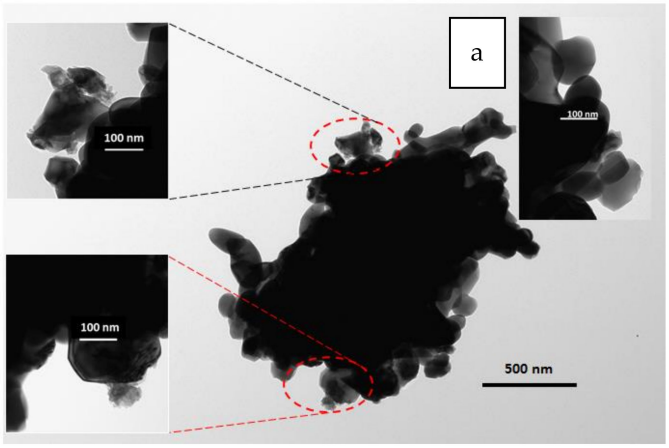

Figure 3. *Cont.*

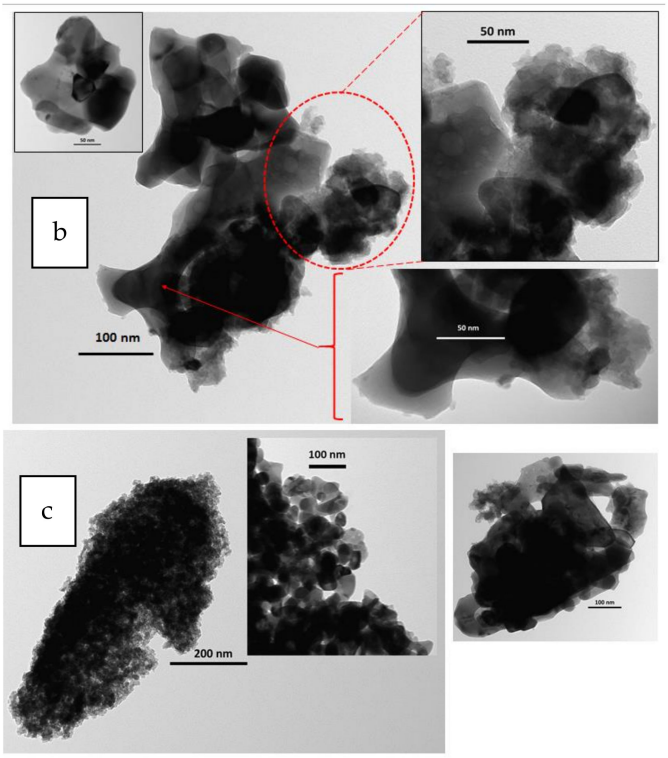

Figure 3. TEM images of $LaFeO_3$ (**a**) of 0.12 $Ni/LaFeO_3$ (**b**) and 0.25 $Ni/LaFeO_3$ (**c**) at different magnifications.

STEM microanalysis of $0.12NiLaFeO_3$ (Figure 4a) evidences the distribution of the different elements constituting the sample. In particular an almost homogenous dispersion of Ni could be evinced, even if there is a low amount of the deposited metal. In the presence of high amount of nickel (Figure 4b), no segregation of Ni occurs, being well distributed also in $0.25Ni/LaFeO_3$.

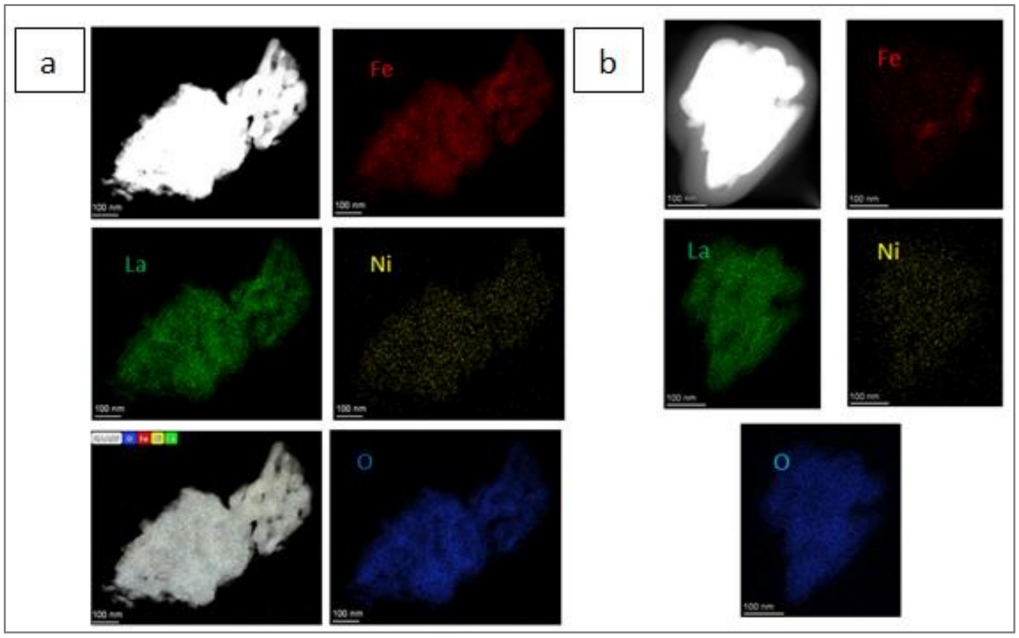

Figure 4. STEM microanalyses of the samples $0.12Ni/LaFeO_3$ (**a**) and $0.25Ni/LaFeO_3$ (**b**).

3.1.6. XPS

The survey spectra of the photocatalysts $LaFeO_3$, 0.12Ni/$LaFeO_3$, and 0.25Ni/$LaFeO_3$ are reported in Figure 5: main peaks related to La, Fe, O and adventitious carbon are evidenced.

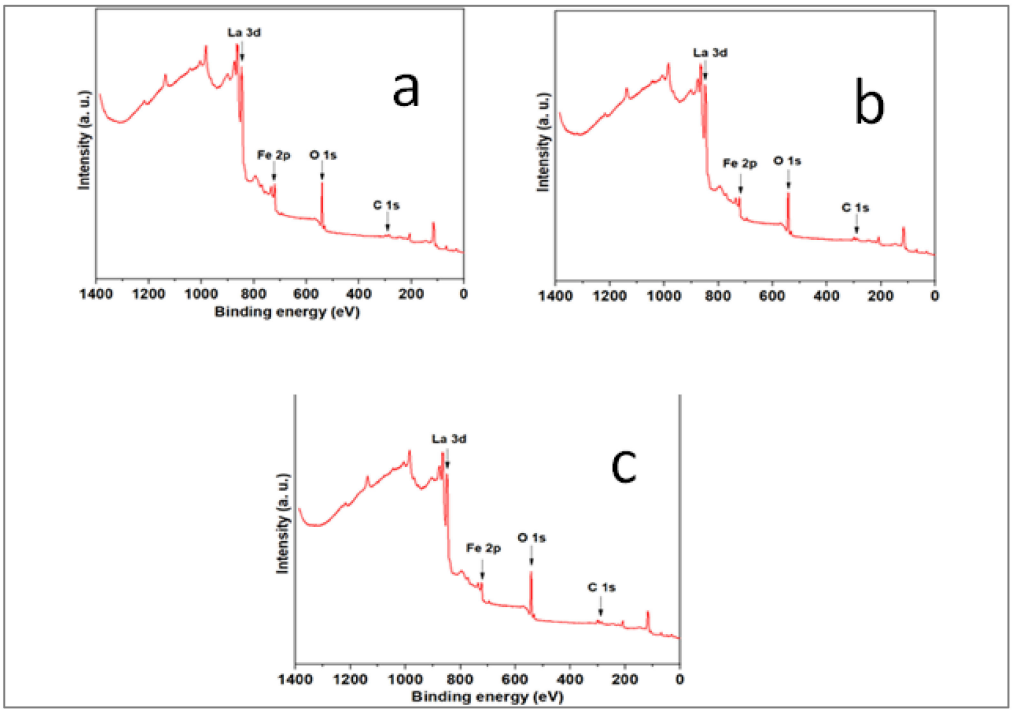

Figure 5. Survey spectra of $LaFeO_3$ (**a**), 0.12 Ni/$LaFeO_3$ (**b**), 0.25Ni/$LaFeO_3$ (**c**).

In the Figure 6a the comparison among the different photocatalyst is shown for the La peaks that show no differences in the La distribution and oxidation state. According to reference [55], the La $3d_{5/2}$ signal has a binding energy of 835.8 eV, separated at 16.8 eV from the La $3d_{3/2}$ signal for lanthanum in 3^+ state (Figure 6a). All samples show a doublet in the $3d_{5/2}$ and $3d_{3/2}$ signals; the signals and the separation of the peaks fits perfectly with the binding energies mentioned. This indicated that the lanthanum state is 3^+ [55]. In the doublets, the peaks with lowest binding energy correspond to La $3d_{5/2}$ and $3d_{3/2}$ signals, and the highest corresponds to satellites signals [56].

In all samples, the Fe 2p spectrum (Figure 6b) has three peaks: Fe $2p_{3/2}$ (709.8 eV), Fe $2p_{1/2}$ (722.6 eV) and a satellite signal (~718 eV), indicating the presence of Fe^{3+}. There is a second signal in Fe $2p_{3/2}$ (708.3 eV) that can be associated with Fe^{2+} [55]. The two peaks from O 1s (Figure 6c) correspond to two kinds of O chemical states, crystal lattice oxygen (OL) and hydroxyl oxygen (OH). The OL signal (528 eV) is attributed to the contribution of La-O and Fe-O in $LaFeO_3$ and the OH signal (530 eV) is closely related to the hydroxyl groups resulting mainly from the chemisorbed water [52]. The proportion of intensity between these peaks change with the %wt. of nickel. As the amount of nickel increases, the intensity of the OH peak increases. Finally, in Figure 6d, the peak at 284.6 eV corresponds to carbon adventitious. The second peak at 288.8 eV may correspond to carbon from carbonates species, generated from the use of citric acid in the synthesis of $LaFeO_3$. There is a doublet peak at lowest binding energy that adventitious carbon. That signals could be attributed to La 4s from La-O and La-Fe bonding. In the 0.12Ni.$LaFeO_3$ and 0.25Ni.$LaFeO_3$ samples, no obvious signs of Ni 2p are seen. The Ni $2p_{3/2}$ peaks may overlap with the La 3d peaks, but no peaks are observed for Ni $2p_{1/2}$ (~872 eV), suggesting the absence of relevant amount of NiO.

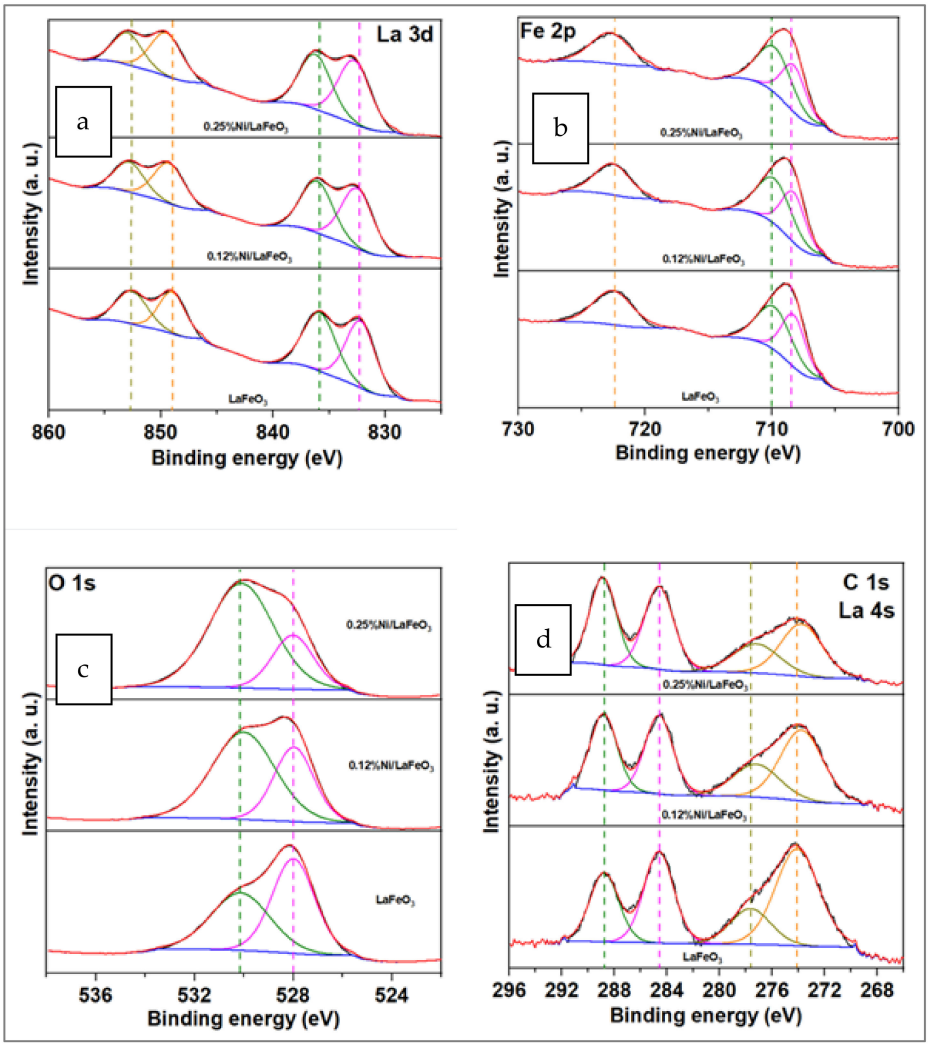

Figure 6. Comparison of XPS spectra of La(3d) (**a**), Fe(2p) (**b**), O(1s) (**c**), and C(1s) (**d**) for $LaFeO_3$, 0.12 $Ni/LaFeO_3$, 0.25$Ni/LaFeO_3$.

3.1.7. XRF

To find further evidence of Ni presence on the $Ni/LaFeO_3$ photocatalysts, XRF analysis was performed and the results are presented in Table 2.

Table 2. XRF results on $LaFeO_3$, 0.12$Ni/LaFeO_3$, 0.25$Ni/LaFeO_3$.

SAMPLE	Ni [%]	Fe [%]	La [%]	O [%]	Ni [Molar Ratio]	Fe [Molar Ratio]	La [Molar Ratio]	O [Molar Ratio]
$LaFeO_3$	-	28	51	20.9	-	0.5	0.37	1.31
0.12$Ni/LaFeO_3$	0.05	31.3	47.1	21.6	$8.5\ 10^{-4}$	0.56	0.34	1.35
0.25$Ni/LaFeO_3$	0.10	31.3	47.1	21.6	$1.7\ 10^{-3}$	0.56	0.34	1.35

Ni is obviously absent on $LaFeO_3$, meanwhile the surface percentage for 0.12$Ni/LaFeO_3$ is found to be 0.05% and double on the sample 0.25$Ni/LaFeO_3$, reaching the value of 0.1%. These values don't agree well with the theoretical content. However, they are present proportionally to the Ni content of the samples. During the reduction with $NaBH_4$, a part of produced Ni metallic nanoparticles possibly loosely contacted with the $LaFeO_3$ surface, and so is lost, leading to a minor content of Ni in the final samples.

3.2. Photocatalytic Hydrogen Production from Glucose Solution

3.2.1. Effect of Ni Amount for the H_2 Production

Figure 7 displays the molecular hydrogen evolution during the UV irradiation time at the spontaneous pH of the solution (pH = 6). For all the investigated photocatalysts, the presence of Ni on perovskite surface resulted in a better activity compared to pure $LaFeO_3$. In particular, it is possible to identify an optimal amount of Ni for which it is possible to obtain the highest hydrogen production. Specifically, the results showed that the optimal Ni amount was equal to 0.12 wt%: with this sample the photocatalytic H_2 production after 4 h of UV irradiation was equal to 2574 µmol/L (corresponding to an H_2 production rate equal to 429 µmol/h/g_{cat}). As confirmed by the characterization results and literature data, the interaction of Ni with the semiconductor surface can cause changes in physical properties, such as particle size, surface structure and distance between conduction and valence bands [57]. It is possible to argue that, when metallic Ni is deposited on the $LaFeO_3$ surface, the migration of excited electrons from the $LaFeO_3$ semiconductor to the metallic Ni occurs until the two Fermi levels are not aligned [58]. At that point, the Schottky barrier formed at the interface between the Ni metal and $LaFeO_3$ acts efficiently as an electron trap and prevents the photogenerated electron-hole recombination: this significantly improves the efficiency of the photocatalytic reaction. Additionally, Ni deposited on $LaFeO_3$ provided active sites for the photoreaction, since the trapped photogenerated electrons are transferred to protons to produce H_2 [57,58].

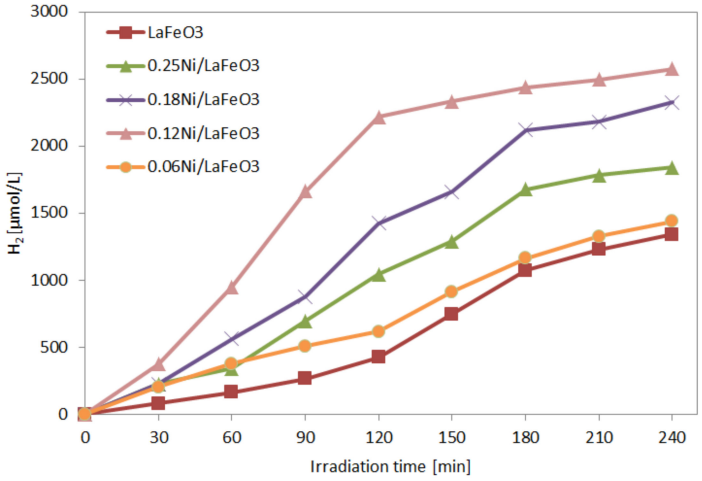

Figure 7. Influence of Ni loading on $LaFeO_3$ for photocatalytic hydrogen production.

3.2.2. Effect of the Catalyst Dosage

The subsequent photocatalytic tests were performed on the catalyst having the best performance in terms of hydrogen production (0.12Ni/$LaFeO_3$). For this catalyst, the dosage was optimized in the range 0.75–3 g/L. The results were reported in Figure 8. The photocatalytic efficiency in the molecular hydrogen production increased as catalyst loading was increased up to 1.5 g/L, after this dosage a decrease in terms of H_2 production was observed.

This result is consistent with the available literature. Indeed an increase in the catalyst dosage beyond the optimal value can cause a worsening of the penetration of light through the solution due to the turbidity of the aqueous suspension [22,59].

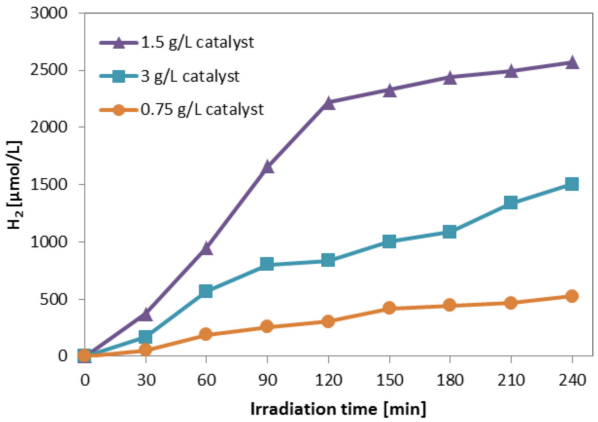

Figure 8. Influence of catalyst dosage on 0.12Ni/$LaFeO_3$ in presence of 1000 pmm of glucose under UV irradiation.

3.2.3. Influence of Initial Glucose Concentration

Figure 9 shows the effect of the initial glucose concentration in aqueous solution on the photocatalytic hydrogen production under UV light. In particular, an increase of the hydrogen production was observed up to 1000 mg/L of initial concentration of glucose, but a further increase in the initial glucose concentration resulted in a decrement in molecular hydrogen production. Some studies reported that the photocatalytic hydrogen production could be affected by the initial concentration of organic substances in aqueous solution following a Langmuir-type isotherm [60–62]. This means that the photocatalytic hydrogen production rate is controlled by saturation of active centers by the adsorbed organic molecules [63]. However, in the present study, the interpretation of the data through a Langmuir-type isotherm does not fit the experimental results obtained, but the existence of an initial optimal glucose concentration is evident. In fact, it was reported that the saturation of the catalysts surface can limit the various reaction steps that lead to the conversion to hydrogen of organic compounds present in the aqueous medium [64–66]. The same behavior was also reported for the photoreforming of glycerol [67,68].

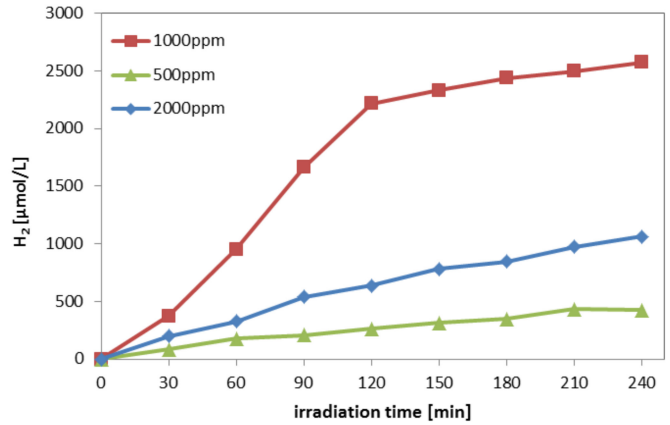

Figure 9. Effect of initial glucose concentration on photocatalytic hydrogen production. Photocatalyst 0.12Ni/$laFeO_3$, 1.5 g/L, under UV irradiation.

3.2.4. Effect of Radical Scavengers

To understand the role of the main reactive species in the photocatalytic molecular hydrogen production from glucose aqueous solution using 0.12Ni/$LaFeO_3$ catalyst, three different experiments in presence of radical scavengers were performed. In particular, isopropyl alcohol, EDTA and potassium dichromate were added to the glucose aqueous solution (1000 ppm of glucose initial concentration) as •OH, h^+ and e^- scavengers, respectively. The obtained results are reported in the Figure 10.

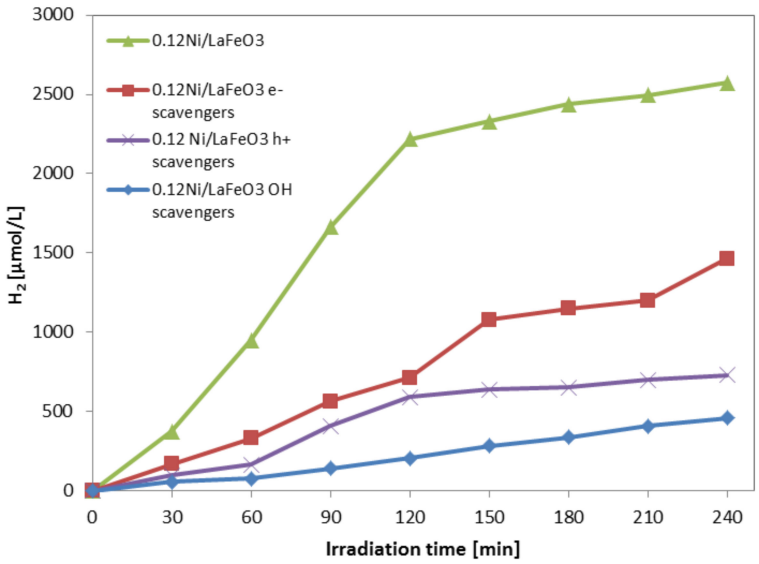

Figure 10. Effect of radical scavengers on photocatalytic performance of 0.12Ni/laFeO$_3$, 1.5g/L, 1000 ppm of glucose, UV irradiation.

The obtained results show that probably, the main contribution to the photocatalytic hydrogen production was given by the •OH. In fact, in presence of •OH scavenger, the hydrogen production decreases significantly. Moreover, also the h^+ seems to play a significant role in the photocatalytic hydrogen production. Finally, electrons seem to have a secondary but not negligible role.

3.2.5. Role of Water in the Reaction Mechanism

To investigate the role of water for the photocatalytic hydrogen production, D_2O was used instead of H_2O during the photocatalytic tests. The results obtained with the D_2O glucose solution compared with H_2O glucose solution are reported in Figure 11. When D_2O was used, the hydrogen production was significantly decreased. In fact, after 4 h of UV radiation, the photocatalytic production of hydrogen in the presence of D_2O was equal to 1394 µmol/L, while in presence of H_2O the production was at its highest value (2573 µmol/L). These results agree with previous literature data [69,70], where it was shown that water should be considered as the primary source for hydrogen production.

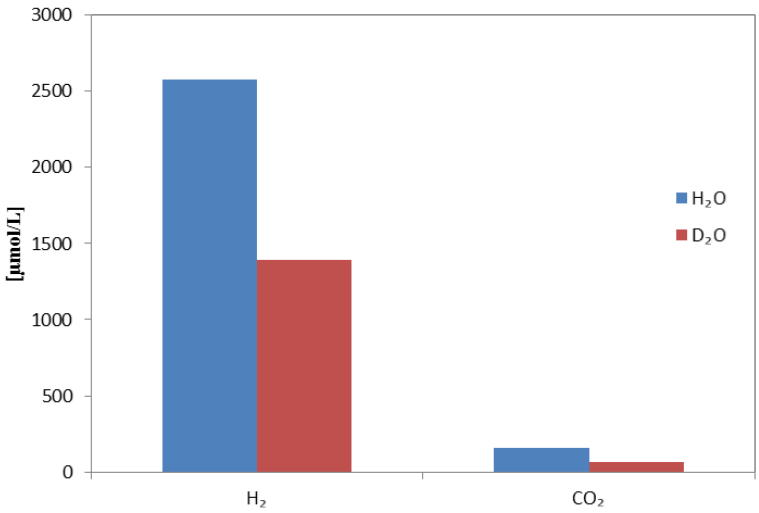

Figure 11. Evolution of gaseous products in photocatalytic reaction of glucose with either H_2O or D_2O. Photocatalyst: 0.12Ni/LaFeO$_3$; catalyst dosage: 1.5 g/L. Initial glucose concentration: 1000 ppm.

These results confirm the fact that during the photocatalytic reforming of glucose, the protons from water molecules were also involved as electron acceptors to produce molecular hydrogen. This finding is consistent with other studies dealing with the photoreforming of formaldehyde [70] and glycerol [67]. Additionally, the production of CO_2 in the presence of water is higher than that obtained in the presence of D_2O, meaning the hydroxyl radicals are the main reactive species involved in the oxidative degradation of intermediates generated from the degradation of glucose. Based on the previous results, a possible reaction mechanism is proposed. Generally, it is possible to consider that the H_2 production derives from the reaction of glucose photoreforming:

$$C_6H_{12}O_6 + 6H_2O = 6CO_2 + 12H_2$$

And from water splitting:

$$2H_2O = 2H_2 + O_2$$

In particular, based on of the experimental results reported above and the data reported in the literature [22] it is possible to define a set of reactions that help to understand the photocatalytic production mechanism of hydrogen starting from aqueous solutions containing glucose.

$$h^+ + H_2O = \bullet OH + H^+ \quad (1)$$

$$h^+ + OH^- = \bullet OH \quad (2)$$

$$H^+ + e^- = 1/2\ H_2 \quad (3)$$

$$RCHO + \bullet OH = RCO\bullet + H_2O \quad (4)$$

or

$$h^+ + RCHO = RCO\bullet + H^+ \quad (5)$$

$$RCO\bullet + H_2O = RCOOH + \bullet H \quad (6)$$

$$RCOOH + \bullet OH = R'\ OH(R''CHO) + CO_2 + \bullet H \quad (7)$$

$$2e^- + 2H^+ = \bullet H + \bullet H \quad (8)$$

$$\bullet H + \bullet H = H_2 \quad (9)$$

where RCHO = $C_6H_{12}O_6$ and RCOOH = $C_6H_{12}O_7$.

The hydroxyl radical •OH plays a key role in the photocatalytic process of hydrogen production; it can be formed by the reaction of H_2O with the h^+ (1) or by the reaction between the h^+ and the OH^- ion (2). So, considering the results reported in Figure 10 it is possible to confirm that: in presence of •OH scavenger, the hydrogen production decrease because the reaction (4) was limited; in presence of electrons e^- scavengers, the limited reaction is (3) where the electrons react with H^+ ions leading to the hydrogen production; in presence of h^+ scavenger it is limited both reaction (1) where the •OH is formed and both the reaction (2) in which the holes react with the OH^- ion to form •OH radical. Based on these reactions, a possible schematic representation of the photocatalytic mechanism is reported in Figure 12.

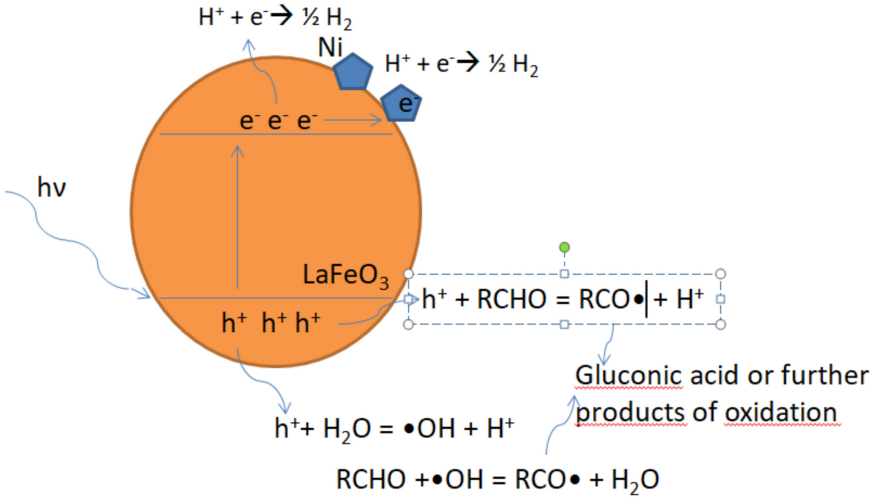

Figure 12. Possible schematic representation of photocatalytic mechanism in presence of Ni/$LaFeO_3$ catalyst.

3.2.6. Stability Tests

To check the stability 0.12 Ni/$LaFeO_3$ sample, the photocatalytic test for hydrogen production was repeated up to four cycles without any step of catalyst regeneration. In particular the suspension was removed from the photoreactor and centrifuged to recover the photocatalyst. After washing with distilled water, 0.12 Ni/$LaFeO_3$ sample was reused without further treatment. The results of stability tests are reported in Figure 13.

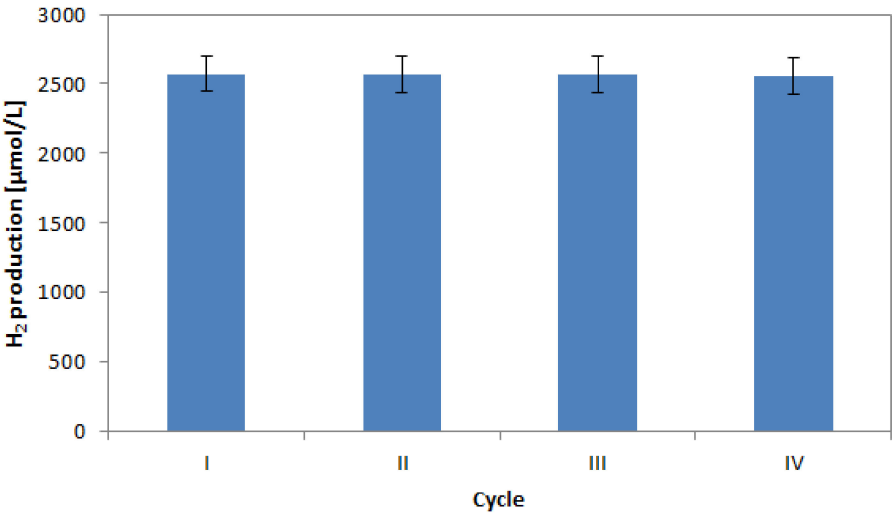

Figure 13. Hydrogen production after 4 h of irradiation time on 0.12 Ni/$LaFeO_3$ catalyst for different cycles.

4. Conclusions

To enhance the photocatalytic performance of $LaFeO_3$ in terms of H_2 production from glucose aqueous solution, an optimized amount of Ni was effectively dispersed on the semiconductor surface. The results of the characterization analyses showed that the inclusion of Ni does not affect the crystal structure of $LaFeO_3$ and does not significantly decrease bandgap energy. However, Ni presence clearly influences the surface structure, provoking smaller particles, higher porosity, and with that, more active sites for reaction. The results of the photocatalytic tests showed that Ni improves the photocatalytic hydrogen evolution activity of $LaFeO_3$. The improvement effect is caused by the fact that Ni nanoparticles can also act as cocatalyst to improve charge separation and transfer. Moreover, the catalyst

dosage was optimized, and the influence of initial glucose concentrations was studied. The results highlighted the existence of an optimal glucose concentration, beyond which the photocatalytic production of hydrogen did not remain constant but worsened. The experiment in presence of radical scavenger demonstrated that hydroxyl radical plays a key role in the photocatalytic process of hydrogen production. Also, the role of H_2O in the photocatalytic production of hydrogen was underlined because when D_2O was used, the rate of hydrogen production was significantly decreased. Finally, this work could highlight the advantages of Ni as a low-cost metal used as a cocatalyst for $LaFeO_3$ in the photocatalytic production of hydrogen from glucose aqueous solutions.

Supplementary Materials: The following are available online at https://www.mdpi.com/article/10.3390/catal11121558/s1, Figure S1: XRD patterns of $LaFeO_3$ and $0.12Ni/LaFeO_3$ samples, Figure S2: Raman spectra of the prepared samples.

Author Contributions: Conceptualization G.I. and V.V.; formal analysis, V.V., D.S. and J.A.N.; investigation, G.I., V.V., F.P. and J.A.N.; data curation, M.C.H., V.V. and D.S.; methodology, M.C.H.; writing—original draft preparation, G.I.; writing—review and editing, G.I., V.V., D.S., F.P. and J.A.N.; visualization, V.V. and M.C.H. All authors have read and agreed to the published version of the manuscript.

Funding: This research was funded by University of Salerno, grant "FORMULAZIONI CATALITICHE INNOVATIVE PER LA SOSTENIBILITÀ ENERGETICA ED AMBIENTALE DEI PROCESSI CHIMICI".

Conflicts of Interest: The authors declare no conflict of interest.

References

1. Moreno, V.C.; Iervolino, G.; Tugnoli, A.; Cozzani, V. Techno-economic and environmental sustainability of biomass waste conversion based on thermocatalytic reforming. *Waste Manag.* **2020**, *101*, 106–115. [CrossRef] [PubMed]
2. Shahabuddin, M.; Krishna, B.B.; Bhaskar, T.; Perkins, G. Advances in the thermo-chemical production of hydrogen from biomass and residual wastes: Summary of recent techno-economic analyses. *Bioresour. Technol.* **2020**, *299*, 122557. [CrossRef] [PubMed]
3. Wang, J.; Liu, H.; Fan, S.; Wang, S.; Xu, G.; Guo, A.; Wang, Z. Dehydrogenation of Cycloalkanes over N-Doped Carbon-Supported Catalysts: The Effects of Active Component and Molecular Structure of the Substrate. *Nanomaterials* **2021**, *11*, 2846. [CrossRef]
4. Abdelhamid, H.; Goda, M.; Said, A. Selective dehydrogenation of isopropanol on carbonized metal–organic frameworks. *Nano-Struct. Nano-Obj.* **2020**, *24*, 100605. [CrossRef]
5. Wang, Y.; Liu, X. Enhanced catalytic performance of cobalt ferrite by a facile reductive treatment for H_2 release from ammonia borane. *J. Mol. Liq.* **2021**, *343*, 117697. [CrossRef]
6. Abdelhamid, H.N. Zeolitic imidazolate frameworks (ZIF-8, ZIF-67, and ZIF-L) for hydrogen production. *Appl. Organomet. Chem.* **2021**, e6319. [CrossRef]
7. Puga, A.V. Photocatalytic production of hydrogen from biomass-derived feedstocks. *Coord. Chem. Rev.* **2016**, *315*, 1–66. [CrossRef]
8. Davis, K.A.; Yoo, S.; Shuler, E.W.; Sherman, B.D.; Lee, S.; Leem, G. Photocatalytic hydrogen evolution from biomass conversion. *Nano Converg.* **2021**, *8*, 1–19. [CrossRef] [PubMed]
9. Fujishima, A.; Honda, K. Electrochemical photolysis of water at a semiconductor electrode. *Nature* **1972**, *238*, 37–38. [CrossRef] [PubMed]
10. Caravaca, A.; Jones, W.; Hardacre, C.; Bowker, M. H_2 production by the photocatalytic reforming of cellulose and raw biomass using Ni, Pd, Pt and Au on titania. *Proc. R. Soc. A Math. Phys. Eng. Sci.* **2016**, *472*, 20160054.
11. Iervolino, G.; Vaiano, V.; Sannino, D.; Rizzo, L.; Galluzzi, A.; Polichetti, M.; Pepe, G.; Campiglia, P. Hydrogen production from glucose degradation in water and wastewater treated by $Ru\text{-}LaFeO_3/Fe_2O_3$ magnetic particles photocatalysis and heterogeneous photo-Fenton. *Int. J. Hydrog. Energy* **2018**, *43*, 2184–2196. [CrossRef]
12. Toe, C.Y.; Tsounis, C.; Zhang, J.; Masood, H.; Gunawan, D.; Scott, J.; Amal, R. Advancing photoreforming of organics: Highlights on photocatalyst and system designs for selective oxidation reactions. *Energy Environ. Sci.* **2021**, *14*, 1140–1175. [CrossRef]
13. Nada, A.A.; Barakat, M.H.; Hamed, H.A.; Mohamed, N.R.; Veziroglu, T.N. Studies on the photocatalytic hydrogen production using suspended modified TiO_2 photocatalysts. *Int. J. Hydrog. Energy* **2005**, *30*, 687–691. [CrossRef]
14. Ni, M.; Leung, M.K.H.; Leung, D.Y.C.; Sumathy, K. A review and recent developments in photocatalytic water-splitting using TiO_2 for hydrogen production. *Renew. Sustain. Energy Rev.* **2007**, *11*, 401–425. [CrossRef]
15. Chiarello, G.L.; Dozzi, M.V.; Selli, E. TiO_2-based materials for photocatalytic hydrogen production. *J. Energy Chem.* **2017**, *26*, 250–258. [CrossRef]
16. Wu, M.-C.; Huang, W.-K.; Lin, T.-H.; Lu, Y.-J. Photocatalytic hydrogen production and photodegradation of organic dyes of hydrogenated TiO_2 nanofibers decorated metal nanoparticles. *Appl. Surf. Sci.* **2019**, *469*, 34–43. [CrossRef]
17. Rusinque, B.; Escobedo, S.; de Lasa, H. Photocatalytic Hydrogen Production Under Near-UV Using Organic Pd-Doped Scavenger Mesoporous TiO_2 and Ethanol as. *Emerg. Trends TiO_2 Photocatal. Appl.* **2020**, *299*. [CrossRef]

18. Rivero, M.J.; Iglesias, O.; Ribao, P.; Ortiz, I. Kinetic performance of TiO_2/Pt/reduced graphene oxide composites in the photocatalytic hydrogen production. *Int. J. Hydrog. Energy* **2019**, *44*, 101–109. [CrossRef]
19. Vaiano, V.; Lara, M.A.; Iervolino, G.; Matarangolo, M.; Navio, J.A.; Hidalgo, M.C. Photocatalytic H_2 production from glycerol aqueous solutions over fluorinated Pt-TiO_2 with high {001} facet exposure. *J. Photochem. Photobiol. A Chem.* **2018**, *365*, 52–59. [CrossRef]
20. Iervolino, G.; Vaiano, V.; Murcia, J.; Rizzo, L.; Ventre, G.; Pepe, G.; Campiglia, P.; Hidalgo, M.; Navío, J.A.; Sannino, D. Photocatalytic hydrogen production from degradation of glucose over fluorinated and platinized TiO_2 catalysts. *J. Catal.* **2016**, *339*, 47–56. [CrossRef]
21. Luna, A.L.; Dragoe, D.; Wang, K.; Beaunier, P.; Kowalska, E.; Ohtani, B.; Bahena Uribe, D.; Valenzuela, M.A.; Remita, H.; Colbeau-Justin, C. Photocatalytic hydrogen evolution using Ni–Pd/TiO_2: Correlation of light absorption, charge-carrier dynamics, and quantum efficiency. *J. Phys. Chem. C* **2017**, *121*, 14302–14311. [CrossRef]
22. Vaiano, V.; Iervolino, G.; Sarno, G.; Sannino, D.; Rizzo, L.; Mesa, J.J.M.; Hidalgo, M.C.; Navío, J.A. Simultaneous production of CH_4 and H_2 from photocatalytic reforming of glucose aqueous solution on sulfated Pd-TiO_2 catalysts. *Oil Gas Sci. Technol. Rev. d'IFP Energ. Nouv.* **2015**, *70*, 891–902. [CrossRef]
23. Murdoch, M.; Waterhouse, G.; Nadeem, M.; Metson, J.; Keane, M.; Howe, R.; Llorca, J.; Idriss, H. The effect of gold loading and particle size on photocatalytic hydrogen production from ethanol over Au/TiO_2 nanoparticles. *Nat. Chem.* **2011**, *3*, 489–492. [CrossRef]
24. Wu, G.; Li, S.; Zhang, C.; Wang, T.; Gong, J. Glycerol steam reforming over perovskite-derived nickel-based catalysts. *Appl. Catal. B Environ.* **2014**, *144*, 277–285. [CrossRef]
25. Chen, S.; Chen, X.; Jiang, Q.; Yuan, J.; Lin, C.; Shangguan, W. Promotion effect of nickel loaded on CdS for photocatalytic H_2 production in lactic acid solution. *Appl. Surf. Sci.* **2014**, *316*, 590–594. [CrossRef]
26. Chen, X.; Chen, W.; Gao, H.; Yang, Y.; Shangguan, W. In situ photodeposition of NiOx on CdS for hydrogen production under visible light: Enhanced activity by controlling solution environment. *Appl. Catal. B Environ.* **2014**, *152*, 68–72. [CrossRef]
27. Chen, X.; Chen, S.; Lin, C.; Jiang, Z.; Shangguan, W. Nickels/CdS photocatalyst prepared by flowerlike Ni/Ni $(OH)_2$ precursor for efficiently photocatalytic H_2 evolution. *Int. J. Hydrog. Energy* **2015**, *40*, 998–1004. [CrossRef]
28. Lin, C.-F.; Chen, X.-P.; Chen, S.; Shangguan, W.-F. Preparation of NiS-Modified Cd1-x Zn x S by a Hydrothermal Method and Its Use for the Efficient Photocatalytic H_2 Evolution. *Acta Phys. Chim. Sin.* **2015**, *31*, 153–158.
29. Chen, X.; Xiong, J.; Shi, J.; Xia, S.; Gui, S.; Shangguan, W. Roles of various Ni species on TiO_2 in enhancing photocatalytic H_2 evolution. *Front. Energy* **2019**, *13*, 684–690. [CrossRef]
30. Hossain, A.; Roy, S.; Sakthipandi, K. The external and internal influences on the tuning of the properties of perovskites: An overview. *Ceram. Int.* **2019**, *45*, 4152–4166. [CrossRef]
31. Arendt, E.; Maione, A.; Klisinska, A.; Sanz, O.; Montes, M.; Suarez, S.; Blanco, J.; Ruiz, P. Structuration of LaMnO3 perovskite catalysts on ceramic and metallic monoliths: Physico-chemical characterisation and catalytic activity in methane combustion. *Appl. Catal. A Gen.* **2008**, *339*, 1–14. [CrossRef]
32. Zhang, L.; Hu, J.; Song, P.; Qin, H.; Jiang, M. Electrical properties and ethanol-sensing characteristics of perovskite La1-XPbxFeO3. *Sens. Actuators B Chem.* **2006**, *114*, 836–840. [CrossRef]
33. Su, H.; Jing, L.; Shi, K.; Yao, C.; Fu, H. Synthesis of large surface area $LaFeO_3$ nanoparticles by SBA-16 template method as high active visible photocatalysts. *J. Nanopart. Res.* **2010**, *12*, 967–974. [CrossRef]
34. Thirumalairajan, S.; Girija, K.; Ganesh, I.; Mangalaraj, D.; Viswanathan, C.; Balamurugan, A.; Ponpandian, N. Controlled synthesis of perovskite $LaFeO_3$ microsphere composed of nanoparticles via self-assembly process and their associated photocatalytic activity. *Chem. Eng. J.* **2012**, *209*, 420–428. [CrossRef]
35. Das, S.; Dutta, S.; Tama, A.M.; Basith, M. Nanostructured $LaFeO_3$-MoS_2 for efficient photodegradation and photocatalytic hydrogen evolution. *Mater. Sci. Eng. B* **2021**, *271*, 115295. [CrossRef]
36. Orak, C.; Yüksel, A. Graphene-supported $LaFeO_3$ for photocatalytic hydrogen energy production. *Int. J. Energy Res.* **2021**, *45*, 12898–12914. [CrossRef]
37. Li, F.T.; Liu, Y.; Liu, R.H.; Sun, Z.M.; Zhao, D.S.; Kou, C.G. Preparation of Ca-doped $LaFeO_3$ nanopowders in a reverse microemulsion and their visible light photocatalytic activity. *Mater. Lett.* **2010**, *64*, 223–225. [CrossRef]
38. Wu, H.; Hu, R.; Zhou, T.; Li, C.; Meng, W.; Yang, J. A novel efficient boron-doped $LaFeO_3$ photocatalyst with large specific surface area for phenol degradation under simulated sunlight. *CrystEngComm* **2015**, *17*, 3859–3865. [CrossRef]
39. Maity, R.; Sheikh, M.S.; Dutta, A.; Sinha, T. Visible light driven photocatalytic activity of granular Pr doped $LaFeO_3$. *J. Electron. Mater.* **2019**, *48*, 4856–4865. [CrossRef]
40. Wang, X.; Qin, H.; Pei, J.; Chen, Y.; Li, L.; Xie, J.; Hu, J. Sensing performances to low concentration acetone for palladium doped LaFeO3 sensors. *J. Rare Earths* **2016**, *34*, 704–710. [CrossRef]
41. Peng, Q.; Shan, B.; Wen, Y.; Chen, R. Enhanced charge transport of $LaFeO_3$ via transition metal (Mn, Co, Cu) doping for visible light photoelectrochemical water oxidation. *Int. J. Hydrog. Energy* **2015**, *40*, 15423–15431. [CrossRef]
42. Gao, K.; Li, S. Multi-modal TiO_2–LaFeO3 composite films with high photocatalytic activity and hydrophilicity. *Appl. Surf. Sci.* **2012**, *258*, 6460–6464. [CrossRef]
43. Sukee, A.; Alharbi, A.A.; Staerz, A.; Wisitsoraat, A.; Liewhiran, C.; Weimar, U.; Barsan, N. Effect of AgO loading on flame-made $LaFeO_3$ p-type semiconductor nanoparticles to acetylene sensing. *Sens. Actuators B Chem.* **2020**, *312*, 127990. [CrossRef]

44. Iervolino, G.; Vaiano, V.; Sannino, D.; Rizzo, L.; Palma, V. Enhanced photocatalytic hydrogen production from glucose aqueous matrices on Ru-doped LaFeO3. *Appl. Catal. B Environ.* **2017**, *207*, 182–194. [CrossRef]
45. Vaiano, V.; Iervolino, G.; Sannino, D. Enhanced photocatalytic hydrogen production from glucose on Rh-doped $LaFeO_3$. *Chem. Eng. Trans.* **2017**, *60*, 235–240. [CrossRef]
46. Chen, W.-T.; Chan, A.; Sun-Waterhouse, D.; Moriga, T.; Idriss, H.; Waterhouse, G.I. Ni/TiO_2: A promising low-cost photocatalytic system for solar H_2 production from ethanol–water mixtures. *J. Catal.* **2015**, *326*, 43–53. [CrossRef]
47. Husin, H.; Pontas, K.; Yunardi, Y.; Salamun, A.; Alam, P.N.; Hasfita, F. Photocatalytic hydrogen production over Ni/La-NaTaO3 nanoparticles from NaCl-water Solution in the presence of glucose as electron donor. *ASEAN J. Chem. Eng.* **2017**, *17*, 27–36. [CrossRef]
48. Vaiano, V.; Iervolino, G.; Sannino, D. Enhanced Photocatalytic Hydrogen Production from Glucose Aqueous Solution Using Nickel Supported on $LaFeO_3$. *Chem. Eng. Trans.* **2021**, *86*, 145–150. [CrossRef]
49. Iervolino, G.; Vaiano, V.; Sannino, D.; Rizzo, L.; Ciambelli, P. Production of hydrogen from glucose by $LaFeO_3$ based photocatalytic process during water treatment. *Int. J. Hydrog. Energy* **2016**, *41*, 959–966. [CrossRef]
50. Kaplan, D.; Alon, M.; Burstein, L.; Rosenberg, Y.; Peled, E. Study of core–shell platinum-based catalyst for methanol and ethylene glycol oxidation. *J. Power Sources* **2011**, *196*, 1078–1083. [CrossRef]
51. Tijare, S.N.; Joshi, M.V.; Padole, P.S.; Mangrulkar, P.A.; Rayalu, S.S.; Labhsetwar, N.K. Photocatalytic hydrogen generation through water splitting on nano-crystalline $LaFeO_3$ perovskite. *Int. J. Hydrog. Energy* **2012**, *37*, 10451–10456. [CrossRef]
52. Parida, K.; Reddy, K.; Martha, S.; Das, D.; Biswal, N. Fabrication of nanocrystalline $LaFeO_3$: An efficient sol–gel auto-combustion assisted visible light responsive photocatalyst for water decomposition. *Int. J. Hydrog. Energy* **2010**, *35*, 12161–12168. [CrossRef]
53. Pawar, G.S.; Elikkottil, A.; Pesala, B.; Tahir, A.A.; Mallick, T.K. Plasmonic nickel nanoparticles decorated on to $LaFeO_3$ photocathode for enhanced solar hydrogen generation. *Int. J. Hydrog. Energy* **2019**, *44*, 578–586. [CrossRef]
54. Phokha, S.; Pinitsoontorn, S.; Maensiri, S.; Rujirawat, S. Structure, optical and magnetic properties of $LaFeO_3$ nanoparticles prepared by polymerized complex method. *J. Sol-Gel Sci. Technol.* **2014**, *71*, 333–341. [CrossRef]
55. Briggs, D. X-ray photoelectron spectroscopy (XPS). *Handb. Adhes* **2005**, 621–622.
56. Feng, Q.; Zhou, J.; Luo, W.; Ding, L.; Cai, W. Photo-Fenton removal of tetracycline hydrochloride using $LaFeO_3$ as a persulfate activator under visible light. *Ecotoxicol. Environ. Saf.* **2020**, *198*, 110661. [CrossRef] [PubMed]
57. Mohamed, R.; Aazam, E.S. H_2 production with low CO selectivity from photocatalytic reforming of glucose on Ni/TiO_2-SiO_2. *Chin. J. Catal.* **2012**, *33*, 247–253. [CrossRef]
58. Linsebigler, A.L.; Lu, G.; Yates, J.T., Jr. Photocatalysis on TiO_2 surfaces: Principles, mechanisms, and selected results. *Chem. Rev.* **1995**, *95*, 735–758. [CrossRef]
59. Akpan, U.G.; Hameed, B.H. Parameters affecting the photocatalytic degradation of dyes using TiO_2-based photocatalysts: A review. *J. Hazard. Mater.* **2009**, *170*, 520–529. [CrossRef]
60. Li, Y.; Lu, G.; Li, S. Photocatalytic hydrogen generation and decomposition of oxalic acid over platinized TiO_2. *Appl. Catal. A: Gen.* **2001**, *214*, 179–185. [CrossRef]
61. Wei, L.F.; Zheng, X.J.; Zhang, Z.H.; Wei, Y.J.; Xie, B.; Wei, M.B.; Sun, X.L. A systematic study of photocatalytic H_2 production from propionic acid solution over Pt/TiO_2 photocatalyst. *Int. J. Energy Res.* **2012**, *36*, 75–86. [CrossRef]
62. Strataki, N.; Bekiari, V.; Kondarides, D.I.; Lianos, P. Hydrogen production by photocatalytic alcohol reforming employing highly efficient nanocrystalline titania films. *Appl. Catal. B Environ.* **2007**, *77*, 184–189. [CrossRef]
63. Tristantini, D.; Ibadurrohman, M. Photocatalytic hydrogen production from glycerol–water mixture over Pt-N-TiO_2 nanotube photocatalyst. *Int. J. Energy Res.* **2013**, *37*, 1372–1381.
64. Ramis, G.; Bahadori, E.; Rossetti, I. Design of efficient photocatalytic processes for the production of hydrogen from biomass derived substrates. *Int. J. Hydrog. Energy* **2021**, *46*, 12105–12116. [CrossRef]
65. Petrosyan, H.; Vanyan, L.; Trchounian, A.; Trchounian, K. Defining the roles of the hydrogenase 3 and 4 subunits in hydrogen production during glucose fermentation: A new model of a H_2-producing hydrogenase complex. *Int. J. Hydrog. Energy* **2020**, *45*, 5192–5201. [CrossRef]
66. Trchounian, K.; Trchounian, A. Hydrogen producing activity by *Escherichia coli* hydrogenase 4 (hyf) depends on glucose concentration. *Int. J. Hydrog. Energy* **2014**, *39*, 16914–16918. [CrossRef]
67. Iervolino, G.; Vaiano, V.; Murcia, J.J.; Lara, A.E.; Hernández, J.S.; Rojas, H.; Navío, J.A.; Hidalgo, M.C. Photocatalytic production of hydrogen and methane from glycerol reforming over Pt/TiO_2–$Nb2O_5$. *Int. J. Hydrog. Energy* **2021**, *46*, 38678–38691. [CrossRef]
68. Ribao, P.; Esteves, M.A.; Fernandes, V.R.; Rivero, M.J.; Rangel, C.M.; Ortiz, I. Challenges arising from the use of TiO_2/rGO/Pt photocatalysts to produce hydrogen from crude glycerol compared to synthetic glycerol. *Int. J. Hydrog. Energy* **2019**, *44*, 28494–28506. [CrossRef]
69. Fujita, S.-i.; Kawamori, H.; Honda, D.; Yoshida, H.; Arai, M. Photocatalytic hydrogen production from aqueous glycerol solution using NiO/TiO_2 catalysts: Effects of preparation and reaction conditions. *Appl. Catal. B Environ.* **2016**, *181*, 818–824. [CrossRef]
70. Belhadj, H.; Hamid, S.; Robertson, P.K.J.; Bahnemann, D.W. Mechanisms of Simultaneous Hydrogen Production and Formaldehyde Oxidation in H_2O and D_2O over Platinized TiO_2. *ACS Catal.* **2017**, *7*, 4753–4758. [CrossRef]